Do Clustering Monoclonal Antibody Solutions Really Have a Concentration Dependence of Viscosity?

Jai A. Pathak,[†‡]* Rumi R. Sologuren,[†‡] and Rojaramani Narwal[†]
[†]Formulations Sciences Department and [‡]Drug Delivery & Device Design Group, MedImmune, Gaithersburg, Maryland

ABSTRACT   Protein solution rheology data in the biophysics literature have incompletely identified factors that govern hydrodynamics. Whereas spontaneous protein adsorption at the air/water (A/W) interface increases the apparent viscosity of surfactant-free globular protein solutions, it is demonstrated here that irreversible clusters also increase system viscosity in the zero shear limit. Solution rheology measured with double gap geometry in a stress-controlled rheometer on a surfactant-free Immunoglobulin solution demonstrated that both irreversible clusters and the A/W interface increased the apparent low shear rate viscosity. Interfacial shear rheology data showed that the A/W interface yields, i.e., shows solid-like behavior. The A/W interface contribution was smaller, yet nonnegligible, in double gap compared to cone-plate geometry. Apparent nonmonotonic composition dependence of viscosity at low shear rates due to irreversible (nonequilibrium) clusters was resolved by filtration to recover a monotonically increasing viscosity-concentration curve, as expected. Although smaller equilibrium clusters also existed, their size and effective volume fraction were unaffected by filtration, rendering their contribution to viscosity invariant. Surfactant-free antibody systems containing clusters have complex hydrodynamic response, reflecting distinct bulk and interface-adsorbed protein as well as irreversible cluster contributions. Literature models for solution viscosity lack the appropriate physics to describe the bulk shear viscosity of unstable surfactant-free antibody solutions.

INTRODUCTION

Because of pioneering breakthroughs in immunology by Köhler and Milstein (1), for which they were coawarded the 1984 Nobel Prize in Physiology and Medicine with Jerne (2), monoclonal antibody (mAb) biologic therapeutics are being applied to treat various diseases. Today, more than one-hundred biologic therapeutics approved by the FDA are prescribed to treat diseases in therapy areas ranging from oncology to inflammation (3). Strides in molecular biology have enabled design of monoclonal antibodies with high affinity and specificity for antigens. These globular protein therapeutics are increasingly formulated in concentrated (molecularly crowded) solutions (4) to ease the dosing regimen for patients. Such molecularly crowded conditions easily render antibody solutions colloidally unstable (5), leading to irreversible clustering. Heavily clustered protein molecules are unacceptable for use as biotherapeutics. Early detection of clustering under storage conditions (2–8°C) remains an outstanding challenge due to thermally driven, slow clustering rates at low temperatures. At high protein concentrations, high shear viscosity (6) and viscoelasticity (7–9) are manifest in crowded solutions (10), wherein excluded volume interactions and other intermolecular interactions are important.

Protein molecules, which are amphiphilic, spontaneously adsorb at the air/water (A/W) interface when dissolved so that hydrophobic patches on their surface can minimize their unfavorable interactions with the strongly polar aqueous medium. Partial unfolding/denaturation of protein molecules occur after monolayer formation at A/W interfaces (11). Protein clusters nucleate at the A/W interface, though the precise mechanism and kinetics of propagation of clustering from the A/W interface to the bulk phase and effects on protein solution rheology (12) and stability (13) are, as of this writing, still poorly understood. Adsorption enables proteins to regain some of the conformational entropy lost upon folding (a compactly packed state) (14), maximizing energetically favorable contacts with the interface (15,16). Surfactant-mediated colloidal stabilization of proteins in solution occurs by preferential adsorption (orogenic displacement) at the air/water (A/W) interface (16) (see *sketch* in Fig. 1). If the surfactant lowers the Gibbs free energy (ΔG) by preferential adsorption at the air/water interface ($\Delta G = \Delta H_{ads} - T\Delta S_{ads}$), the system reaches a thermodynamically favored state (ΔH_{ads} and ΔS_{ads} denote the enthalpy and entropy difference, respectively, and T denotes absolute temperature). Preferentially adsorbed surfactant molecules essentially keep protein molecules away from the A/W interface.

For reasons discussed above, A/W interface adsorption of protein molecules complicates measurement of viscosity of all surfactant-free protein solutions in the presence of an A/W interface. Torsional rheometry with cone-plate geometry on these systems measures bulk viscous dissipation and the elasticity/stiffness of the adsorbed protein film at the A/W interface, as both contribute to measured torque in rheometers. Sharma et al. (17) have recently quantified the effects of surface area/volume ratio and A/W interfacial
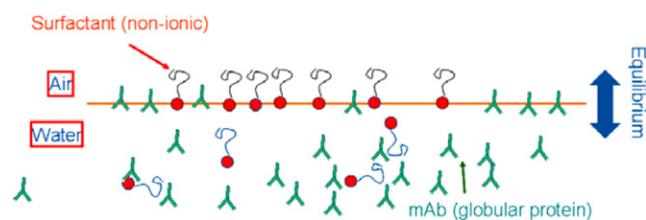
FIGURE 1 Schematic of preferential adsorption of surfactant at air/water interface (orogenic displacement). Surfactant molecules (*red*) have a hydrophobic head and hydrophilic tail, and monoclonal antibody molecules (*green*) have a Y-shape (Fab and Fc domains).

adsorption on the apparent bulk shear viscosity of surfactant-free bovine serum albumin (BSA) solutions. They have shown that adsorbed protein at the A/W interface causes an apparent rise in low shear viscosity and apparent yield behavior in the cone-plate geometry in dilute solutions. Both these artifacts are mitigated in the double gap (hollow bob in a cup) geometry, as the exposed interface area is compensated by increased bulk contribution due to larger contact area between the hollow bob and the test fluid. They added Polysorbate (PS)-80 surfactant to the BSA solution and saw consistent data in the cone and double gap geometries as PS-80 prefers to adsorb to the A/W interface over BSA, and lowers the interfacial viscoelasticity, as compared to a BSA-saturated interface.

Adsorption (A/W interface) effects on low shear viscosity of protein solutions have been investigated but, to the best of our knowledge, as of the time of this writing, no systematic studies are available that address the influence of protein clusters on the shear viscosity of surfactant-free protein solutions. When protein solutions become colloidally unstable, they form both reversible (equilibrium) and irreversible (nonequilibrium) clusters that span a wide range of lengthscales, from oligomers on the order of 10–100 nm to microscopic clusters (0.1–100 μm) and precipitated visible clusters (>100 μm) (18). Self-assembled clusters are governed by equilibrium thermodynamics, whereas irreversible clusters are highly nonequilibrium. Concentration dependence of protein solution viscosity and the mutual diffusion coefficient reflect both hydrodynamic and thermodynamic contributions at high concentrations. Clustering effects on viscosity are poorly understood. Here it is quantitatively demonstrated that, in addition to interface adsorption effects (17), irreversible clusters nontrivially increase solution viscosity in a surfactant-free Immunoglobulin (IgG1) solution. Although suspension rheology (19) models can be reconciled with this result, it has important implications for studies of protein solution rheology in biophysics and its applications in the biotechnology industry.

MATERIALS AND METHODS

A fully humanized IgG1 mAb (manufactured by MedImmune, Gaithersburg, MD) was employed. It was prepared by cloning and expression

from mammalian cells, followed by purification; the final concentration by tangential (cross) flow filtration was used. This mAb, which has mass-averaged molar mass 148 KDa, was dissolved in a pH 6.0 buffer containing 10 mm Histidine and 150 mM NaCl. Because the pH was below the mAb iso-electric point (pI = 8.15), the protein molecules were positively charged. The density of the fully formulated solution with [mAb] = 100 g L^{-1} at 23°C, as measured with a model No. DMA 4500M densitometer (Anton Paar, Ashland, VA), was 1.037 g cc^{-1} (data not shown). Measurements on a surfactant-laden positive control system were taken by adding 0.03% (w/v) Polysorbate 80 N.F. (Lot No. K0958; J. T. Baker/Avantor, Phillipsburg, NJ) to the mAb solution. Protein concentration was determined by A$_{280}$ UV absorption measurements at wavelength (λ) = 280 nm. Most rheology data were taken at 10 g L^{-1} and 107 g L^{-1} concentrations; measurements were also made on solutions diluted with buffer to 25, 50, and 70 g L^{-1}. All solutions were stored at ~5°C.

Measurements on surfactant-laden solutions and measurements on all protein concentrations were conducted using a cone-plate geometry of radius (R_{CONE}) 20 mm, 1° angle, and 350 μL sample volume at 5°C and 23°C with an MCR-301 torsional rheometer (Anton Paar) which detects torque (T) in the range 0.1 μN·m $\leq T \leq$ 200 mN·m. Motor adjustment and tool inertia correction were performed before measurements, and the residual T with air was $\leq \pm$ 0.02 μN·m. Rheology measurements on the 107 g L^{-1} solution were performed in double gap geometry (Cat. No. DG26.7; Anton Paar) to mitigate protein interface adsorption effects with a sample volume of 3.8 mL. The length and radius of the bob were L_{BOB} = 40 mm and outer R_{BOB} = 13.3 mm, respectively. All measurements were started at 10^3 s^{-1}, ramped down to 10^{-1}–10^{-2} s^{-1}, and ramped back up to 10^3 s^{-1} to erase any shear history and also because crowded protein solutions often possess a yield stress (20) (discussed below).

Samples free of visible air bubbles were prepared at a cone-plate separation of 250 μm with a flashlight before setting the final measurement gap (96 μm) in the cone-plate geometry, while bubble-free samples were prepared in the double gap geometry by careful pipetting and visual inspection of the limited exposed surface. A hood covered the cone-plate geometry to mitigate evaporation. Although no such cover was available for the double gap geometry, visual inspection confirmed that no significant evaporation occurred over experimental timescales (45 min, maximum). The rheometer was programmed to let T reach steady state by allowing 60 s at each shear rate; 5–6 data points were acquired in each decade of shear rate. Rheometer calibration was checked using a mineral-oil-based viscosity standard (N7.5; Lot No. 09101a; Cannon Instruments, State College, PA) of certified standard viscosity 11.5 mPa·s at 20°C. The rheometer measured 11.6 mPa·s, signifying 1.3% uncertainty. Disposable 1 mL Tuberculin Slip Tip syringe and 3 mL luer lock syringe (BD Labware, Franklin Lakes, NJ) and low protein binding Millex-GV 0.22 μm sterile filters (Cat. No. SLGV013SL; Millipore, Cork, Ireland) with Durapore Poly(Vinylidene Fluoride) membranes (Millipore) were used for filtration into cone-plate and double gap geometries, respectively.

High shear pressure-driven flow rheometry was done at 24 ± 1°C in a 50 μm deep × 6.2 mm long × 3.1 mm wide microfluidic slit (m-VROC, or viscometer-rheometer-on-a-chip; Rheosense, San Ramon, CA) equipped with three pressure sensors flush-mounted along the axis of the chip for axial pressure drop, $\Delta P(x)$, measurements. The sensors' full-scale deflection is 800 KPa, and accuracy is 1% of full-scale deflection. The minimum and maximum bounds of the dynamic range in shear stress are 22.7 and 2270 Pa, respectively, while the sampling time is 15 ms. The shear stress (τ) was calculated from the slope (β) of the linear $\Delta P(x)$, channel width, w, and height, h:

$$\tau_w = -\beta \frac{wh}{2(w+h)}.$$

The two-dimensional Weissenberg-Rabinowitsch correction (21) was applied to determine the true wall-shear rate $\dot{\gamma}_{true}$ for rate-dependent viscosity in non-Newtonian fluids, for which $\dot{\gamma}_{true}$ differs from the apparent shear rate,

$$\dot{\gamma}_{app} = 6Q/wh^2 : \dot{\gamma}_{true} = \frac{\dot{\gamma}_{app}}{3}\left[2 + \frac{d\ln\dot{\gamma}_{app}}{d\ln\tau}\right],$$

where Q denotes the volumetric flow rate, and viscosity is calculated using $\tau_w = \eta\dot{\gamma}_{true}$.

A/W interface rheology of the mAb solution was measured on a stress-controlled TA AR-G2 rheometer (TA Instruments, New Castle, DE) using a double-wall ring fixture (22). This rheometer measures torque in the range $0.01\ \mu$N-m $\leq T \leq 200$ mN-m. Rotational mapping of the optical encoder and bearing friction correction were performed as prescribed by the manufacturer, and the residual T with air was within limits ($\leq \pm 0.01\ \mu$N·m). Surface flow curve data were acquired on a freshly loaded sample that was withdrawn from the bulk fluid inside a conical tube using a 25 mL serological pipette and a handheld Falcon Express dispenser (BD Labware). A 12 mL sample volume was dispensed into a Teflon double-wall Couette cell while avoiding bubbles. Surface flow curves were first measured between 10^2 and 10^{-3} s^{-1}, and then ramped to 10^2 s^{-1}. Inertia effects were seen above 10^2 s^{-1}, which necessitated terminating experiments. The interface age was ~5 min at the start of the experiment. No hysteresis effects were observed in the surface viscosity.

MicroFlow Imaging (MFI; Protein Simple, Toronto, Canada) was done on a DPA 4100 flow microscope (4.88 × objective; field of view of 1.747 mm height × 1.404 mm width with a depth of field of 400 μm claimed by the vendor, Brightwell Technologies, Ottawa, Canada (23)). The flow rate is 0.22 mL min^{-1} in a 40 mm wide × 1.3 mm long × 400 μm flow cell. Although confinement-induced cluster-wall interaction effects for large clusters (>50 μm) can be a concern, shear-induced dispersion and migration (19) effects on imaging were mitigated in the MFI by the large depth of field.

UV-detector-based size-exclusion chromatography (SEC) was performed using an 1100 series HP-SEC (Agilent Technologies, Santa Clara, CA) loaded with a model No. G3000SWXL column (25 nm pore size; Tosoh Bioscience, San Francisco, CA). A series of 25 μL injections was performed on samples diluted to 10 g L^{-1} concentration to prevent column overloading and detector saturation.

Dynamic light scattering (DLS) was performed on precentrifuged samples (to remove air bubbles) on a DynaPro Plate Reader (Wyatt Technology, Santa Barbara, CA) equipped with a detector that detects light ($\lambda = 830$ nm) scattered at an angle (2θ) = 158°, corresponding to a scattering wavevector (q) = $4\pi n\sin(\theta)/\lambda$ = 0.02 nm^{-1} (20.0 μm^{-1}). Here, $n = 1.357$ is the mAb solution refractive index at 23°C, which was measured with a Refracto 30GS refractometer (Mettler Toledo, Columbus, OH). Because scattering angle determines lengthscales probed by DLS, this large scattering angle precludes resolution at lengthscales exceeding $l^* = 2\pi/20.0\ \mu$m^{-1} = 0.314 μm. DLS data (24) are plotted as autocorrelation function of scattered light intensity fluctuations, $g^{(2)}(\underline{q},\tau) - 1$ versus time:

$$g^{(2)}(q,\tau) \equiv \frac{\left\langle I\left(\underline{q},0\right)I\left(\underline{q},\tau\right)\right\rangle}{\left\langle I\left(\underline{q}\right)\right\rangle^2}.$$

The ordinate seen later in Fig. 6 is

$$g^{(2)}(q,\tau) - 1 = \left[g^{(1)}(q,\tau)\right]^{(2)} = \left[g^{(2)}(q,\tau) - 1\right]^{0.5}$$
$$= f^M(q,\tau),$$

which is the Fourier transform of the density-density correlation function, $G(r,t)$ (25),

$$G(r,t) = \left\langle\rho\left(\underline{r} = 0, t = 0\right)\rho\left(\underline{r},t\right)\right\rangle.$$

RESULTS AND DISCUSSIONS

Bulk rheology of mAb solution

As the origins of this study, apparent viscosity (η) versus shear rate ($\dot{\gamma}$) flow curve data on solutions with protein concentrations between 10 g L^{-1} and 107 g L^{-1}, are shown in Fig. 2 a. Although the low shear rotational rheometry data agreed reasonably well with the high shear micro-slit rheometry data, they revealed a perplexing conundrum: below $\dot{\gamma}$ ~10^2 s^{-1}, the viscosity of the 10 g L^{-1} solution apparently exceeded that of the concentrated 107 g L^{-1} solution. However, the viscosity increase was not an artifact
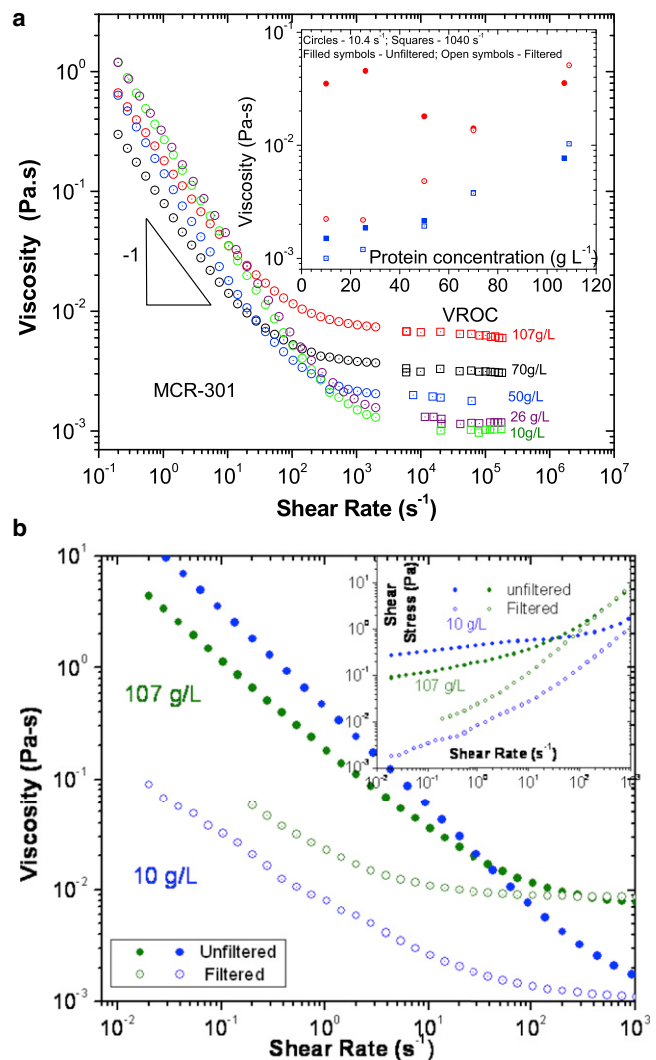

FIGURE 2 (*a*) Cone-plate rheometry data of as-is solutions (taken from the storage refrigerator and allowed to equilibrate to 23°C in the rheometer). Data are shown on the stock solution (107 g L^{-1}) and diluted (10, 26, 50, and 70 g L^{-1}) solutions. (*Inset*) Viscosity values at 10.4 s^{-1} (*circles*) and 1040 s^{-1} (*squares*) as a function of protein concentration. (*Solid* and *open symbols*) Unfiltered and filtered solutions, respectively. (*b*) Flow curves of unfiltered solution (*solid symbols*) and filtered solution (*open symbols*) at 23°C for 10 g L^{-1} and 107 g L^{-1} mAb solutions. (*Inset plot*) Shear stress versus shear rate.

of torque measurement in the stress-controlled MCR-301 rheometer, as the torques corresponding to elevated viscosity were well above the rheometer's torque resolution limit. At high shear rates, all solutions displayed the infinite shear rate plateau with a characteristic infinite shear rate viscosity, η_∞, which scales monotonically with concentration.

Because proteins possess charge and size characteristic of colloids (5), the Krieger-Dougherty model (26) (Eq. 1) has been suggested to apply to the composition dependence of protein solution viscosity (8,9,17),

$$\frac{\eta}{\eta_s} = \left(1 - \frac{\varphi_{mon}}{\varphi_m}\right)^{-[\eta]\varphi_m} \quad (1)$$

In Eq. 1, η_s, ϕ_{mon}, ϕ_m, and $[\eta]$ denote solvent viscosity, protein monomer volume fraction, maximum packing volume fraction, and intrinsic viscosity, respectively. For proteins, the ϕ value must be calculated carefully to account for hydration. The viscosity of solutions of varying [mAb] is plotted in Fig. 2 a (inset) at two shear rates (10.4 s^{-1} and 1040 s^{-1}). At 10.4 s^{-1}, the viscosity apparently displayed a spurious peak at [mAb] = 25 g L^{-1}, while the viscosity monotonically increased with [mAb] at 1040 s^{-1}, as expected. Clearly, the measured η {[mAb]} at 10.4 s^{-1} violates the Krieger-Dougherty model, which sensibly predicts that η monotonically increases with ϕ_{mon}. The Ross-Minton model (27,28) also predicts η to monotonically increase with ϕ_{mon}. While the data of Fig. 2 a (inset) violate all such models, the conclusions from Fig. 2 a are model-independent.

Because the data in Fig. 2 a were acquired on surfactant-free solutions taken straight from the container stored at 5°C for several months, it was hypothesized that apparent non-monotonic dependence of viscosity on concentration arose due to irreversible clusters. Therefore, to exclude these large clusters, solutions were filtered through 0.22 μm filters directly onto the plate in the cone-plate geometry immediately before flow-curve measurement. Flow curves on filtered solutions (Fig. 2 b) revealed low shear rate viscosity that was an order-of-magnitude smaller compared to unfiltered solutions. Moreover, the viscosity of the filtered 10 g L^{-1} solution remained consistently smaller than that of the filtered 107 g L^{-1} solution across all shear rates measured, as expected. Filtration restored monotonic dependence of viscosity on [mAb], in accord with Eq. 1 (see Fig. 2 a, inset). A relevant observation in this context is that although the viscosity of the filtered solutions was much smaller than the unfiltered solutions, at asymptotically high shear rates, they coincided with each other.

The low shear rate viscosity in Fig. 2 a showed a slope (ν) = −1 in the double logarithmic flow curve. This characteristic slope signifies yielding (solid-like rheological behavior), as the shear stress (σ) becomes independent of shear rate $\dot{\gamma}$, because $\sigma = \eta\dot{\gamma}$ (20,21). When $\eta \sim \dot{\gamma}^{-1}$, then

$\sigma \sim \dot{\gamma}^0$. Below the yield stress, the system effectively has infinite viscosity. Shear thinning (associated with liquid rheology, and thus distinct from yield) is characterized by $\nu_B > -1$ (typically ~ -0.8). The subscript B denotes bulk here. Origins of solid-like rheology in this mAb solution where electrostatic interactions are screened due to counterions from added salt are indeed puzzling, as long-range interactions would be required to create some kind of network-like structure (20) that is overcome to enable momentum transfer with finite viscosities. After filtration, ν_B value increased, signifying transition from yield to shear thinning. However, even filtered concentrated solutions at [mAb] = 70 and 107 g L^{-1} retained $\nu_B = -1$, suggesting that the A/W interface film caused yield. Of course, clusters smaller than 0.22 μm could also have contributed to the observed yield.

Flow curves in Fig. 2 were undoubtedly impacted by macromolecular adsorption at the A/W interface (17). In Fig. 3, data taken in the cone-plate and double gap geometries for the 107 g L^{-1} solution are compared. Viscosity measured by the double gap geometry was an order-of-magnitude lower than in the cone-plate geometry at shear rate < 1 s^{-1}. Viscosity measured immediately after filtration of the solution into the cup of the double gap geometry showed a further, though admittedly smaller, drop due to exclusion of cluster species larger than 0.22 μm. At 1 s^{-1}, the viscosity difference pre- and postfiltration in the double gap geometry was approximately twofold. Minimal impact of the A/W interface in the double gap geometry has been proposed by Sharma et al. (17) on the basis of their calculations of ratio of the surface drag and the subphase (bulk) drag (Boussinesq number (29), Bo), which depends on the surface shear viscosity (η_s), bulk viscosity (η), and the characteristic measurement geometry lengthscale (l): $Bo = \eta_s/l\eta$. The ratio of the area of the fixture in contact
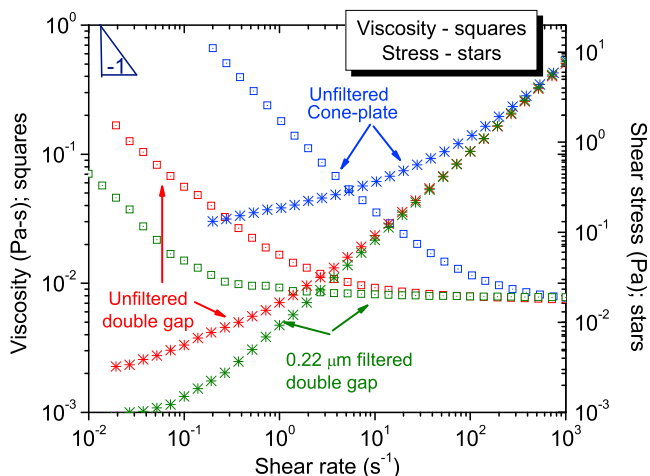

FIGURE 3 Flow curves at 23°C of unfiltered mAb solution (107 g L^{-1}) in the cone-plate geometry (blue squares), unfiltered solution in the double gap (red squares), and filtered solution in the double gap geometry (green squares). (Asterisks; same color code applies) Shear stress.

with the subphase fluid (A_{SUB}) and the perimeter of the probe in contact with the interface (P_{INT}) defines l; $l = A_{SUB}/P_{INT}$. Typically, for $Bo \gg 1$, surface stress dominates, whereas for $Bo \ll 1$, subphase stress dominates the rheometric measurement. Interfacial and bulk contributions will be parameterized after a discussion of interfacial rheology data.

Further indirect evidence for the role of the clusters was provided by flow-curve data on a PS-80-spiked mAb solution wherein the concentration of all other components was held constant. Because PS-80 preferentially adsorbs to the interface, it mitigates protein clustering. Low shear viscosity data in Fig. 4 were unaffected by filtration, as PS-80 can prevent large clusters from forming, in qualitative agreement with the report of Patapoff and Esue (30). Data at 5°C are shown here as this cone-plate geometry gave poor signal/noise at low shear rates of interest at 23°C. Lowering temperature does not negate the generality of this result, which could have been equivalently established by using a larger cone to improve torque ($T \sim R^4$) (21). In Fig. 4, $\nu_B > -1$, signifying that shear thinning, and not yielding, caused viscosity drop. The addition of PS-80 created a transition from solid-like to liquidlike behavior in the low shear rate regime.

Biophysical (DLS and SEC) characterization

The biophysical characterization experiments that led to the conclusion that exclusion of irreversible clusters also caused viscosity decrease after filtration in the double gap geometry will now be discussed. As good practice, protein solution rheology studies should be accompanied by minimal biophysical measurements (size exclusion, dynamic light scattering, etc.) to characterize reversible clusters along with visualization of larger irreversible clusters.
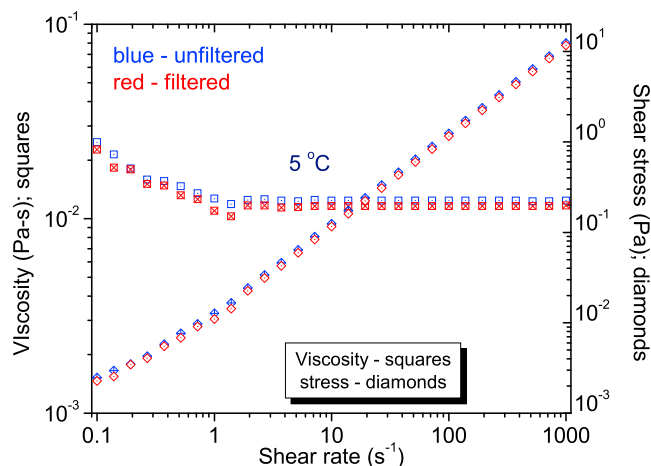

FIGURE 4 Effects of filtration on the flow curves of surfactant-spiked antibody solution ([mAb] = 100 g L^{-1}) at 5°C. (*Squares* and *diamonds*) Viscosity and shear stress, respectively. (*Blue* and *red symbols*) Unfiltered and filtered solutions, respectively.

HP-SEC measurements (Fig. 5) on mAb solutions revealed that the ratio of monomer (98%) to reversible clusters (2%) remained invariant upon filtration. Because SEC separates species by hydrodynamic size, larger-molecular-weight cluster species are eluted first, followed by monomers. Of course, as expected from principles of suspension hydrodynamics (19), the contribution of clusters to viscosity depends on cluster size and volume fraction. The contribution of reversible clusters will scale with their effective volume fraction in the system, which is small here. Because the effective reversible cluster volume fraction remained constant, their contribution to the low shear viscosity of the system also remained invariant after filtration.

DLS data on unfiltered and filtered solutions were fitted to a single exponential time decay function with amplitude (A) and baseline (B):

$$g^{(2)}(q, \tau) - 1 = A \exp(-\tau_m t) + B. \qquad (2)$$

In Eq. 2, τ_m denotes the relaxation time of the protein monomer, which is the time taken by a monomer to diffuse through a distance equal to its own characteristic size. Monomers were the smallest scatterers in the system, and hence diffused fastest. Filtration barely impacted the diffusion timescale, confirming that monomer diffusion was manifested in the exponential relaxation (Fig. 6). A much lower-amplitude relaxation was seen at longer timescales, possibly from larger reversible clusters, so their relaxation was also detected:

$$D_s = \frac{k_B T}{6\eta \pi R_h}. \qquad (3)$$

DLS is, of course, primarily a powerful dynamic probe, though it is applied pervasively to sizing. These are interrelated by Eq. 3, the Stokes-Einstein-Sutherland (31,32) equation, which follows from the fluctuation-dissipation theorem (25). It relates the dilute solution self-diffusion coefficient ($D_s = \tau q^2$) to matrix viscosity η, hydrodynamic radius R_h, and thermal energy ($k_B T$), where k_B denotes Boltzmann's constant. The value R_h was calculated to be ~6.5 nm (see Table 1), slightly exceeding literature estimates of 5.5 nm for IgG1 molecules (33). This discrepancy may have arisen from the skewing of the size distribution to larger lengthscales because of larger reversible species within DLS temporal resolution. The value τ_m increases in concentrated formulations as molecular crowding retards diffusion.

When probed at $q = 0.02$ nm^{-1}, both the relaxation timescale τ and the lengthscale R_h remained invariant upon filtration at constant [mAb], leading to the inference that the lengthscale of the species responsible for the low shear viscosity rise (impacted by filtration) exceeded l^* (0.31 μm). Reversible protein clusters (much smaller than l^*) did not account for the viscosity rise and apparent nonmonotonic composition dependence of viscosity in Fig. 2 a. Larger
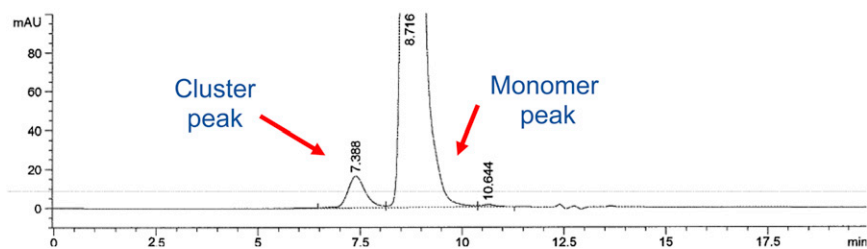
FIGURE 5 HP-SEC peaks of filtered and unfiltered solutions showing the presence of peaks due to the monomer and reversible clusters. Monomer content is 98% in both cases. Data are only shown on the unfiltered solution for clarity and space. Filtered solutions gave quantitatively identical HP-SEC data as unfiltered solutions.

irreversible clusters were thus a plausible explanation for the low shear viscosity discrepancy seen in Fig. 2 a. Although [mAb] decrease due to adsorption on the filter membrane could also lead to viscosity decrease, it was checked after filtration, and the observed 3–4 mg/mL drop was well within the uncertainty associated with the A_{280} assay and in accord with the performance of these low protein binding filters. Moreover, small drops in [mAb] could not have quantitatively accounted for the order-of-magnitude low shear viscosity drops seen after filtration. Furthermore, although slow syringe filtration subjects the protein molecules to shear flow at high rates ($10^3 - 10^5 \, s^{-1}$), these rates are benign to the conformational stability of protein molecules, and should not destabilize the folded state for small strains (34). The scaling model proposed by Jaspe and Hagen (34) predicts that extremely high shear rates ($\sim 10^7 \, s^{-1}$) are necessary to denature globular protein molecules. Therefore, filtration neither causes denaturation nor induces clustering. The interfacial contribution to the measured stress also remains unperturbed by filtration, as the interfacial stress is determined by the protein surface concentration and the thickness of the surface layer. Because the bulk solution concentration remains essentially unchanged upon filtration, the interfacial tension at the air/water interface remains effectively constant. Protein adsorption, which governs surface film thickness, is homologous in molecular dimensions (35) and not in bulk composition. The interfacial contribution to stress should also remain unchanged upon filtration. Finally, electrostatic effects cannot explain the data in Fig. 3. These factors motivated the flow microscopy and interfacial rheology experiments, described next.

Flow microscopy: morphological characterization of irreversible clusters

To characterize irreversible clusters, flow visualization (36), a powerful experimental tool in multiphase fluid mechanics, was applied. When refractive index contrast is sufficient, suspended clusters can be distinguished from the matrix by optical microscopy. MFI data clearly documented the presence of large irreversible clusters in unfiltered solutions (Fig. 7 a) that were excluded after filtration through a 0.22 μm filter (Fig. 7 b), accounting partially for the postfiltration viscosity drop in Figs. 2 and 3. The number of 2 μm-size clusters in Fig. 7 a exceeded that in Fig. 7 b by a factor of ~200. MFI data for a surfactant-spiked solution (Fig. 7 c)

also showed that the cluster count in this size range is much smaller than in the surfactant-free case (Fig. 7 a).

The overall system viscosity reflects the sum total response from monomers in bulk solution, monomers adsorbed to the interface, reversible clusters, and also suspended irreversible clusters. Clearly, such clustering systems have a dual solution-suspension nature: the dissolved monomers and higher-order clusters reflect the response of the protein solution, while the clusters seen by MFI form a suspension. Without detection and characterization of the microscopic clusters, it would be erroneously concluded that measured viscosity merely reflects the hydrodynamic response of dissolved species. As of this writing, no theoretical models are available for the viscosity of such hybrid solution-suspension systems.

In sheared cluster suspensions, a convective flow field competes with thermal-energy-driven Brownian motion. Clusters of size much larger than 1 μm are non-Brownian. Flow anisotropically aligns and orients clusters with the flow direction as shear rate increases, whereas Brownian motion tends to isotropically and randomly disperse them. This competition is parameterized by the dimensionless Peclèt number (Pe), the ratio of shear stress and Brownian stress. It is a dimensionless shear rate and a metric of departure from equilibrium:
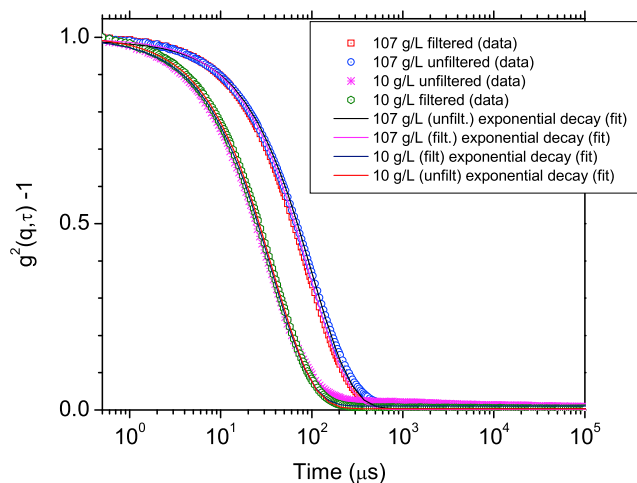

FIGURE 6 Autocorrelation function of intensity fluctuations (from dynamic light scattering) of filtered and unfiltered antibody solutions. (Symbols) Experimental data. (Solid lines) Exponential fits (Eq. 2).

TABLE 1 Monomer diffusion time (τ_m) and hydrodynamic radius (R_h) of filtered and unfiltered protein solutions at 25°C

System	τ_m, Monomer diffusion time (ms)	Hydrodynamic radius, R_h (nm) (Eq. 3)
107 g L^{-1} unfiltered	100 ± 0.2	—
107 g L^{-1} filtered	93.9 ± 0.1	—
10 g L^{-1} unfiltered	37.7 ± 0.06	6.8 ± 0.04
10 g L^{-1} filtered	36.3 ± 0.1	6.5 ± 0.1

R_h data for 107 g L^{-1} solution are not reported because the Stokes-Einstein-Sutherland equation (Eq. 3) is not valid at high concentrations.

$$Pe = \frac{\sigma}{\frac{k_{B}T}{a^3}} = \frac{\eta\dot{\gamma}a^3}{k_{B}T}. \tag{4}$$

Here, a denotes the cluster diameter (assumed spherical). Simple scaling and dimensional analysis predict that the dimensionless viscosity of a Brownian hard-sphere particle dispersion: $\eta/\eta_s = f(Pe, \phi_p)$. For $Pe \gg 1$, hydrodynamic (shear) effects overwhelm Brownian effects and suspended clusters/dissolved molecules become oriented with the flow direction. Conversely, Brownian motion dominates hydrodynamic effects when $Pe \ll 1$ where the suspension exists in near-equilibrium.

Cluster sizes obtained from MFI data were converted into equivalent circular diameter, and number-averaged equivalent circular diameter, $\langle d \rangle_N$, was used to approximate a in Eq. 4:

$$\langle d \rangle_N = \frac{\sum\limits_i n_i d_i^2}{\sum\limits_i n_i d_i}. \tag{5}$$

This approximate Pe calculation was done assuming that a remained uninfluenced by the flow field; clearly, this assumption could fail at very high shear rates where flow can break up clusters. For filtered and unfiltered solutions, $Pe \gg 1$ (Fig. 8) and increased with shear rate, as expected. Pe values showed that hydrodynamic effects remained important even at the lowest shear rates measured. Whereas Brownian contributions were amplified at lower shear rates, they were not responsible for viscosity changes after filtration. Although hydrodynamic effects clearly played a role in increasing viscosity in the low shear regime, the volume fraction of the clusters detected by MFI was low (~1%), and it could not alone explain the order of magnitude decrease in viscosity after filtration in the double gap geometry. This motivated measurement of the A/W interfacial rheology of the mAb solution to quantify the interfacial contribution to the increased bulk low shear rate viscosity (17).

A/W interface rheology of mAb solution

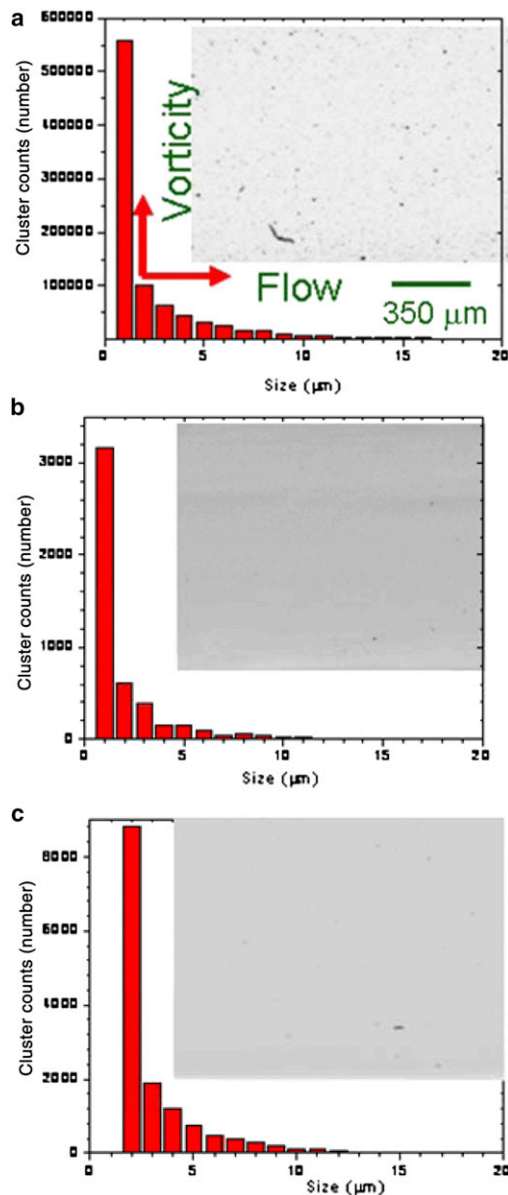Measured A/W interfacial viscosity and interfacial shear stress data for the mAb solution are compared to the

FIGURE 7 Cluster size distribution (MFI data) of (*a*) unfiltered surfactant-free, (*b*) filtered surfactant-free, and (*c*) unfiltered surfactant-laden antibody solutions with representative optical micrographs (*inset*). Scale bar for micrograph in panel *a* also applies to panels *b* and *c*.

data of Sharma et al. (17) on 100 g L^{-1} BSA in PBS (pH = 7.4) in Fig. 9. The interfacial viscosity of the mAb solution was an order-of-magnitude larger than BSA. Moreover, both solutions yielded at the interface: slope ν_S in double logarithmic plot of interfacial viscosity versus shear rate = −1. The subscript S refers to surface here. The interfacial yield stress, $\tau_{S,y}$, for the mAb and BSA were 6.5×10^{-3} Pa·m and 1.5×10^{-3} Pa·m, respectively, which signifies that the mAb solution formed a much stiffer film at the A/W interface than the BSA solution. Stiffer films make larger interfacial contribution to the torque measured by a rheometer in bulk rheology, and hence to the bulk shear
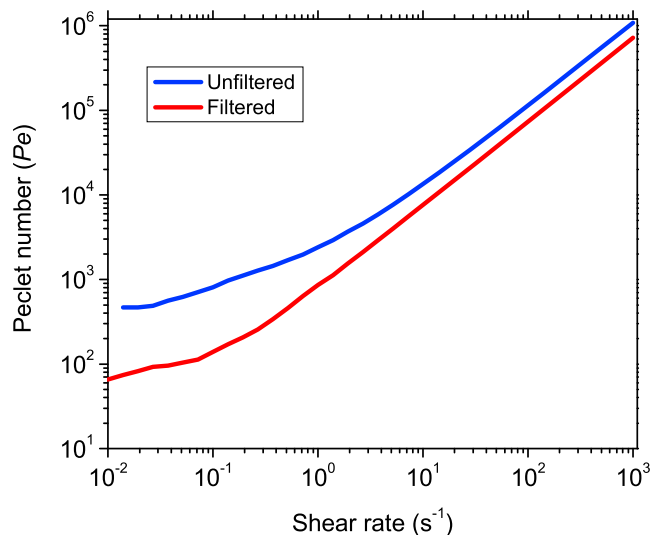
FIGURE 8 Peclèt number calculated from MFI data for unfiltered and filtered solutions, plotted versus shear rate.

viscosity of the mAb solution. Using the bulk η and interfacial η data at numerically equal bulk and surface shear rate $= 10^{-2}$ s^{-1}, the Boussinesq number (Bo) was calculated (Table 2) for the double gap geometry,

$$l \approx \frac{A_{\text{SUB}}}{P_{\text{INT}}} \approx \frac{2 \times 2\pi R_{\text{BOB}} \times L_{\text{BOB}}}{2 \times 2\pi R_{\text{BOB}}} = L_{\text{BOB}}. \quad (6)$$

For the cone-plate geometry,

$$l \approx \frac{A_{\text{SUB}}}{P_{\text{INT}}} \approx \frac{\frac{2}{3} \times \pi R_{\text{CONE}}^2}{2\pi R_{\text{CONE}}} = \frac{R_{\text{CONE}}}{3}. \quad (7)$$

Interfacial effects are about even with bulk effects for the mAb solution in double gap geometry: $Bo = 0.5$ and 3.0 for double gap and cone-plate geometries, respectively.
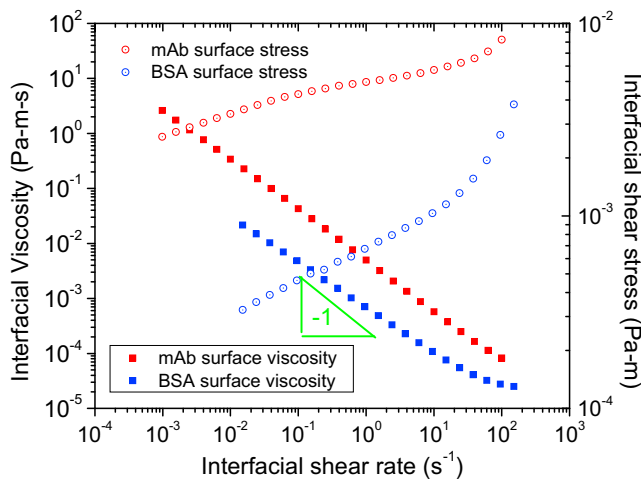

FIGURE 9 Surface flow curve (surface viscosity and surface shear stress) of mAb solution, compared to BSA data of Sharma et al. (17).

Sharma et al. (17) derived the interfacial contribution to the bulk shear viscosity measured via the torque (T_{DG}) measured in a double gap geometry in terms of $\tau_{S,Y}$ and η_∞:

$$\eta\left(\dot{\gamma}\right) = \frac{T_{DG}\left(\dot{\gamma}\right)}{4\pi R_B^2 L_B \dot{\gamma}} \approx \eta_B + \frac{\eta_S\left(\dot{\gamma}\right)}{l_{DG}} \approx \eta_\infty + \frac{\tau_{S,Y}}{L_B \dot{\gamma}}. \quad (8)$$

Although the double gap geometry mitigated interface effects, reflected in lower Bo relative to the cone-plate geometry, the interfacial contribution in this work never became negligible compared to the bulk: Bo always remained O (1–10). This result differs from that of Sharma et al. (17) because the characteristic length $l = L_B$ of their double gap geometry was larger (59.5 mm, compared to 40 mm here), giving lower Bo. The higher $\tau_{S,Y}$ for mAb solution and smaller L_B for the double gap geometry used here lead to the conclusion that interfacial adsorption effects on bulk viscosity (Eq. 8) predominated contribution of irreversible clusters in the increase of the low-shear-regime viscosity. Proteins have been shown to form stiff elastic films at the A/W interface (37,38), whose contribution to the bulk viscosity in surfactant-free systems should not be neglected.

As seen in Fig. 3, the larger drop in viscosity is contributed by mitigation of interfacial contributions in switching from the cone to the double gap geometry, with a significantly smaller drop contributed by the exclusion of irreversible clusters (Fig. 7 a) after clustering. The cluster contribution to viscosity was significantly smaller than the interfacial contribution due to the low-cluster volume fraction. Interfacial component to the measured torque (hence bulk shear stress and bulk viscosity) was smaller in the double gap geometry here, but remained significant nevertheless. These conclusions are different from those of Sharma et al. (17), who have only identified interfacial adsorption as a factor responsible for artificially high low-shear viscosity of surfactant-free protein solutions. It has been shown here that clusters also contribute to this phenomenon, and need to be characterized and accounted for.

DISCUSSION

These data, which clearly show that both clustering and mAb interfacial adsorption, led to increased apparent viscosity in surfactant-free mAb solutions, motivate the need to measure and report the rheology of clustering systems and protein solutions across as broad and practical a range of shear rates as possible, while carefully accounting for both interfacial and cluster contributions. Torsional rheometry data on surfactant-free antibody/protein solution should be treated with caution, and supporting interfacial rheology data may be needed to interpret the bulk rheology data. Literature reports often provide protein solution viscosity

TABLE 2   Comparison of Boussinesq number in cone-plate and double gap geometry for mAb solution and BSA data

System	Bulk viscosity @ 0.01 s^{-1} (25°C) Pa-s	A/W Interfacial viscosity @ 0.01 s^{-1} (23°C); Pa-m-s	*Bo*: 40 mm cone-plate geometry	*Bo*: Double gap geometry
100 mg/mL BSA solution in PBS	0.175	0.02	17 (l = 6.7 mm)	1.8 (l = 59.5 mm)[a]
104 mg/mL mAb solution in 25 mM histidine buffer	10.0	0.2	3.0 (l = 6.7 mm)	0.5 (l = 40 mm)

Note that l for the double gap geometry in Sharma et al. (17) was 59.5 mm. Boussinesq numbers have been calculated here using characteristic l values as provided in Sharma et al. (17).
[a]Data from Sharma et al. (17).

only at a single shear rate, typically 10^3 s^{-1} (39,40) as protein solutions reach the infinite shear rate plateau by ~10^3 s^{-1}. Ultrasonic rheometry operates only at a single frequency, and thus it is not a spectroscopy (41). Hence, it would completely miss the presence of large protein clusters that relax at much lower shear rates/frequencies than smaller monomers.

Some reports have provided complete flow curves (7,8,28) whereas others (42,43) have provided only the 10^3 s^{-1} datum out of a measured flow curve. Using a viscosity datum at 10^3 s^{-1}, Yadav et al. (39) have recently postulated that "although reversible self-association would increase the solution viscosity at concentrations where equilibrium favors the self-associated state, irreversible clustering resulting in a phase-separated solute precipitation will lead to a decrease in solution viscosity." Although this assertion is intuitively appealing, inasmuch as protein depletion from solution into a condensed phase would cause viscosity to decrease, there is nevertheless a tradeoff between viscosity decrease due to monomer loss from solution and viscosity increase due to formation of suspended protein clusters at nonvanishing cluster volume fractions and interfacial effects. The formation of irreversible clusters neither requires much protein nor does it change the bulk protein concentration appreciably (experimentally verified here).

These experimental results on clustering effects leading to enhanced viscosity also agree qualitatively with both experimental and simulation results. Liu et al. (44) and Choi and Park (45) have already demonstrated increased system viscosity in bovine serum IgG clusters by heating above the melting (unfolding) temperature, T_m = 75°C and clustering driven by 10 M urea-induced unfolding of BSA. Their results support the conclusions drawn here that irreversible protein clusters increase system viscosity. Choi and Park's data are especially significant as they performed viscometry in a custom-fabricated microfluidic channel, which forms a closed system with no A/W interface and found that bulk nonnative clusters raised the viscosity by ~30% relative to the native state after unfolding-driven clustering, which contradicts the conjecture of Yadav et al. (39). Finally, the Stokesian dynamics simulation results of Silbert et al. (46) on the rheology of concentrated clustering colloidal suspensions and experimental data of Buscall et al. (47) on depletion-flocculated colloidal suspensions also agree qualitatively with the data here that show viscosity increase due to irreversible clusters.

CONCLUSIONS

Apparent nonmonotonic concentration dependence of viscosity in a crowded surfactant-free IgG1 solution has been resolved by filtering irreversible protein clusters that were detected by flow visualization. Double gap rheometry, wherein interfacial adsorption artifacts are mitigated but still remain nonnegligible here, showed a significant low shear viscosity drop after filtration of clusters, which restored the expected monotonic composition dependence of viscosity. Reversible cluster species, whose size/relaxation time and effective volume fraction remained unperturbed by filtration, coexisted with protein monomers in solution.

The findings of Sharma et al. (17) regarding the significant interfacial contribution to the measured bulk shear viscosity in a surfactant-free protein solution have been confirmed. This antibody solution showed yield (solid-like) behavior at the air/water interface, measured using a double-wall ring in a stress-controlled rheometer. Boussinesq number (surface stress to subphase stress ratio) calculations have shown that the double gap geometry also senses interfacial contributions here due to a smaller bob length (40 mm) in this work, compared to 59.5 mm in Sharma et al. (17). Moreover, it has been demonstrated that protein clusters can also contribute to the low-shear-rate viscosity of unstable protein solutions. Great caution should be exercised in the measurement of surfactant-free protein/antibody solution rheology in torsional (rotational) viscometers, as the stiff interfacial film and cluster formation can contribute to the measured viscosity.

In addition to intermolecular interactions (electrostatic, excluded volume, van der Waals forces, solvation and hydrophobic interactions), instability-induced clusters and protein adsorption at interfaces create hydrodynamic and interfacial contributions to protein solution rheology, respectively. Only low-shear rheology measurements are sensitive to the presence of clusters in unstable protein solutions and to interfacial effects. Molar mass (12), concentration (12), and net charge/charge distribution (37) considerations, though important, are insufficient to understand all features of the rheology of clustering systems that have dual protein solution and cluster suspension nature. Minimal biophysical and cluster characterization are necessary for rationalizing rheology data in clustering protein solutions. Theoretical models of viscosity of clustering protein solutions as a

function of concentration and size of monomers, reversible and irreversible clusters, are currently unavailable as of this writing. This difficult problem spans several orders of magnitude in length- and timescales. Models of composite time and shear rate dependence of the viscosity of clustering systems will help correlate kinetic protein stability with solution viscosity.

REFERENCES

1. Köhler, G., and C. Milstein. 1975. Continuous cultures of fused cells secreting antibody of predefined specificity. *Nature.* 256:495–497.

2. The Nobel Prize in Physiology or Medicine. 1984. http://www.nobelprize.org/nobel_prizes/medicine/laureates/1984/.

3. Leader, B., Q. J. Baca, and D. E. Golan. 2008. Protein therapeutics: a summary and pharmacological classification. *Nat. Rev. Drug Discov.* 7:21–39.

4. Shire, S. J. 2009. Formulation and manufacturability of biologics. *Curr. Opin. Biotechnol.* 20:708–714.

5. DeYoung, L. R., A. L. Fink, and K. A. Dill. 1993. Aggregation of globular proteins. *Acc. Chem. Res.* 26:614–620.

6. Shire, S. J., Z. Shahrokh, and J. Liu. 2004. Challenges in the development of high protein concentration formulations. *J. Pharm. Sci.* 93:1390–1402.

7. Brownsey, G. J., T. R. Noel, …, S. G. Ring. 2003. The glass transition behavior of the globular protein bovine serum albumin. *Biophys. J.* 85:3943–3950.

8. Parker, R., T. R. Noel, …, S. G. Ring. 2005. The nonequilibrium phase and glass transition behavior of β-lactoglobulin. *Biophys. J.* 89:1227–1236.

9. Lonetti, B., E. Fratini, …, P. Baglioni. 2004. Viscoelastic and small neutron scattering studies of concentrated protein solutions. *Phys. Chem. Chem. Phys.* 6:1388–1395.

10. Zhou, H.-Z., G. Rivas, and A. P. Minton. 2008. Macromolecular crowding and confinement: biochemical, biophysical and potentially physiological consequences. *Annu. Rev. Biophys.* 37:375–397.

11. Tronin, A., T. Dubrovsky, …, C. Nicolini. 1996. Role of protein unfolding in monolayer formation on air/water interface. *Langmuir.* 12:3272–3275.

12. Tanford, C. 1961. Physical Chemistry of Macromolecules. John Wiley, New York.

13. Frokjaer, S., and D. E. Otzen. 2005. Protein drug stability: a formulation challenge. *Nat. Rev. Drug Discov.* 4:298–306.

14. Adamson, A. W., and A. P. Gast. 1997. Physical Chemistry of Surfaces. John Wiley, New York.

15. Tilton, R. D., C. R. Robertson, and A. P. Gast. 1990. Lateral diffusion of BSA at the solid-liquid interface. *J. Colloid Interface Sci.* 137: 192–203.

16. Mackie, A. R., A. P. Gunning, …, V. J. Morris. 1999. Orogenic displacement of protein from the air/water interface by competitive adsorption. *J. Colloid Interface Sci.* 210:157–166.

17. Sharma, V., A. Jaishankar, …, G. H. McKinley. 2011. Rheology of globular proteins: apparent yield stress, high shear rate viscosity and interfacial viscoelasticity of BSA solutions. *Soft Matter.* 7:5150–5160.

18. Narhi, L. O., J. Schmit, …, D. Sharma. 2012. Classification of protein aggregates. *J. Pharm. Sci.* 101:493–498.

19. Guazzelli, E., and J. F. Morris. 2012. A Physical Introduction to Suspension Dynamics. Cambridge University Press, Cambridge, UK.

20. Larson, R. G. 1998. The Structure and Rheology of Complex Fluids. Oxford University Press, Oxford, UK.

21. Macosko, C. W. 1994. Rheology: Principles, Measurements and Applications. Wiley-VCH, New York.

22. Vandebril, S., A. Franck, …, J. A. Vermant. 2010. A double-wall ring for interfacial shear rheometry. *Rheologica Acta.* 49:131–144.

23. King, G. G., and S. E. LeBlanc. May 27, 2008. U.S. Patent No. 7,379,577. Method and apparatus for particle measurement employing optical imaging. Brightwell Technologies, Stittsville, Ontario, Canada.

24. Zemb, T., and P. Lindner. 2002. Neutrons, X-Rays and Light Scattering Methods Applied to Soft Condensed Matter. North Holland Press, Amsterdam.

25. McQuarrie, D. A. 2000. Statistical Mechanics. University Science Books, Herndon, VA.

26. Krieger, I. M., and T. J. Dougherty. 1959. A mechanism for non-Newtonian flow in suspensions of rigid spheres. *Trans. Soc. Rheol.* 3:137–152.

27. Ross, P. D., and A. P. Minton. 1977. Hard quasispherical model for the viscosity of hemoglobin solutions. *Biochem. Biophys. Res. Commun.* 76:971–976.

28. Minton, A. P. 2012. Hard quasispherical particle models for the viscosity of solutions of protein mixtures. *J. Phys. Chem. B.* 116:9310–9315.

29. Edwards, D. A., H. Brenner, and D. A. Wasan. 1991. Interfacial Transport Processes and Rheology. Butterworth Heinemann, London, UK.

30. Patapoff, T. W., and O. Esue. 2009. Polysorbate 20 prevents the precipitation of a monoclonal antibody during shear. *Pharm. Dev. Technol.* 14:659–664.

31. Einstein, A. 1905. On the molecular kinetic theory of the thermally driven motion of suspended particles in stationary fluids [Über die von der molekularkinetischen Theorie der Wärme geforderte Bewegung in ruhenden Flüssigkeiten suspendierten Teilchen]. *Annalen der Physik.* 322:549–560.

32. Sutherland, W. 1905. A dynamical theory of diffusion for non-electrolytes and the molar mass of albumin. *Philos. Mag.* 9:781–785.

33. Jøssang, T., J. Feder, and E. Rosenqvist. 1988. Photon correlation spectroscopy of human IgG. *J. Protein Chem.* 7:165–171.

34. Jaspe, J., and S. J. Hagen. 2006. Do protein molecules unfold in a simple shear flow? *Biophys. J.* 91:3415–3424.

35. Krishnan, A., C. A. Siedlecki, and E. A. Vogler. 2003. Traube rule interpretation of protein adsorption at the air/water interface. *Langmuir.* 19:10342–10352.

36. Adrian, R. J. 1991. Particle imaging techniques for experimental fluid mechanics. *Annu. Rev. Fluid Mech.* 23:261–304.

37. Sankaranarayanan, K., A. Dhathathreyan, …, R. Miller. 2012. Interfacial viscoelasticity of myoglobin at air/water and air/solution interfaces: role of folding and clustering. *J. Phys. Chem. B.* 116:895–902.

38. Bolanos-Garcia, V. M., A. Renault, and S. Beaufils. 2008. Surface rheology and adsorption kinetics reveal amphiphilicity, interfacial activity and stability of human exchangeable apolipoproteins. *Biophys. J.* 20:10159–10167.

39. Yadav, S., T. M. Laue, …, S. J. Shire. 2012. The influence of charge distribution on self-association and viscosity behavior of monoclonal antibody solutions. *Mol. Pharm.* 9:791–802.

40. Du, W., and A. M. Klibanov. 2011. Hydrophobic salts markedly diminish viscosity of concentrated protein solutions. *Biotechnol. Bioeng.* 108:632–636.

41. Saluja, A., A. V. Badkar, …, D. S. Kalonia. 2007. Ultrasonic storage modulus as a novel parameter for analyzing protein-protein interactions in high protein concentration solutions: correlation with static and dynamic light scattering measurements. *Biophys. J.* 92:234–244.

42. Salinas, B. A., H. A. Sathish, …, T. W. Randolph. 2010. Understanding and modulating opalescence and viscosity in a monoclonal antibody formulation. *J. Pharm. Sci.* 99:82–93.

43. Kanai, S., J. Liu, …, S. J. Shire. 2008. Reversible self-association of a concentrated monoclonal antibody solution mediated by Fab-Fab interaction that impacts solution viscosity. *J. Pharm. Sci.* 97:4219–4227.

44. Liu, C., C. Vailhe, …, Q. Min. 2009. A simple and reproducible approach to characterize protein stability using rheology. *Int. J. Pharm.* 374:1–4.

45. Choi, S., and J.-K. Park. 2010. Microfluidic rheometer for characterization of protein unfolding and aggregation in microflows. *Small.* 6:1306–1310.

46. Silbert, L. E., J. R. Melrose, and R. C. Ball. 1999. The rheology and microstructure of concentrated, clustered colloids. *J. Rheol.* 43:673–700.

47. Buscall, R., J. I. McGowan, and A. J. Morton-Jones. 1993. The rheology of concentrated dispersions of weakly attracting colloidal clusters with and without wall slip. *J. Rheol.* 37:621–641.